Polarized optical reflectance and electronic structure of the charge-density-wave materials η- and γ-Mo_4O_{11}

Z. Zhu, S. Chowdhary, V. C. Long, and J. L. Musfeldt
Department of Chemistry, State University of New York at Binghamton, Binghamton, New York 13902-6016

H.-J. Koo and M.-H. Whangbo
Department of Chemistry, North Carolina State University, Raleigh, North Carolina 27695

X. Wei
National High Magnetic Field Laboratory, Florida State University, Tallahassee, Florida 32306

H. Negishi and M. Inoue
Graduate School of Advanced Sciences of Matter, Hiroshima University, Higashi-Hiroshima 739-8526, Japan

J. Sarrao and Z. Fisk
National High Magnetic Field Laboratory, Florida State University, Tallahassee, Florida 32306
(Received 7 June 1999; revised manuscript received 10 November 1999)

We report the polarized optical reflectance spectra of η- and γ-Mo_4O_{11} as a function of temperature and magnetic field. Excitations are assigned and analyzed based upon electronic band-structure calculations. The 300 K spectra of η- and γ-Mo_4O_{11} show charge transfer transitions (O $2p \rightarrow$ Mo $4d$) near 4 eV, intraband ($d \rightarrow d$) transitions at $\sim$1.5 eV, and a free carrier response at lower energy. The intraband ($d \rightarrow d$) transition shows strong and unusual anisotropy in the b and c directions, which is directly attributable to the dispersion relations of the lower-lying d-block bands. The effect of charge density wave formation on the optical properties of η- and γ-Mo_4O_{11} is discussed and compared with related materials. The magnetic field dependence of the optical constants is determined for η-Mo_4O_{11} and discussed in terms of field effects on the nesting vector and Fermi surface.

I. INTRODUCTION

Low-dimensional metallic oxides have been the subject of sustained interest during the past decade.[1–4] Many of these solids display electronic instabilities, which lead to a superstructure modulation and a charge-density-wave (CDW) ground state. The general mechanism of CDW formation in these materials is well known.[5] Strong electron-phonon interactions leading to a CDW may remove the free carriers completely (or reduce their number) and open an energy gap at the Fermi level, thus causing a metal $\rightarrow$ insulator (or metal $\rightarrow$ metal) phase transition.

η- and γ-Mo_4O_{11}, along with other low-dimensional molybdenum and tungsten oxides, have been studied extensively as model CDW materials.[1–3,6] Both compounds exhibit quasi-two-dimensional (Q2D) metallic properties at high temperature. The η and γ phase compounds have monoclinic and orthorhombic structures, respectively,[7,8] as shown in the insets of Fig. 1. Both consist of infinite slabs of distorted MoO_6 octahedra, parallel to the bc plane, fused together by MoO_4 tetrahedra. The conduction electrons are confined in the octahedral slabs, which leads to a partially filled conduction band in the bc plane and a Q2D electronic structure. The difference in the η and γ phase compounds lies in the arrangement of successive MoO_6 slabs; the adjacent slabs have the same orientation in η-Mo_4O_{11}, but are mirror images with respect to the bc plane in γ-Mo_4O_{11}.

η-Mo_4O_{11} undergoes two separate incommensurate CDW transitions at 109 and 35 K, which have been confirmed by dc resistivity, thermopower, and magnetic susceptibility measurements.[9,10] The x-ray and electron diffraction studies show that the first CDW transition ($T_{c1}=109$ K) is accompanied by a structural modulation with the nesting vector $q_1=(0,\ 0.23b^*,\ 0)$; the second CDW transition ($T_{c2}=35$ K) is accompanied by $q_2=(?,\ 0.42b^*,\ 0.28c^*)$.[10] In this material, holes as well as electrons contribute to conduction processes,[11,12] and the Fermi surfaces have a Q2D shape (cylindrical along the a^* axis), as determined by magnetoresistivity and Hall effect studies.[13,14] The CDW transitions in η-Mo_4O_{11} are essentially due to nesting of the ''hidden'' one-dimensional bands,[6] which originate from the conducting chains along b, $b \pm c$ directions. Furthermore, de Haas-van Alphen oscillations indicate that small, highly two-dimensional electron and hole Fermi surfaces persist at low-temperature.[15] These Fermi surfaces lead to unusual physical properties at high magnetic fields, including a Landau transition near 19 T,[13] the recently reported bulk quantum Hall effect,[16,17] and a plastic deformation under an applied field.[18] The well-defined quantum Hall signatures below 10 T in η-Mo_4O_{11} are thought to originate in exchange between the mobile carriers and the localized CDW condensate.[16] At high field, a magnetic-field-induced semimetal $\rightarrow$ semiconductor transition in η-Mo_4O_{11} is attributed to a quantum limit effect, where the conduction and valence

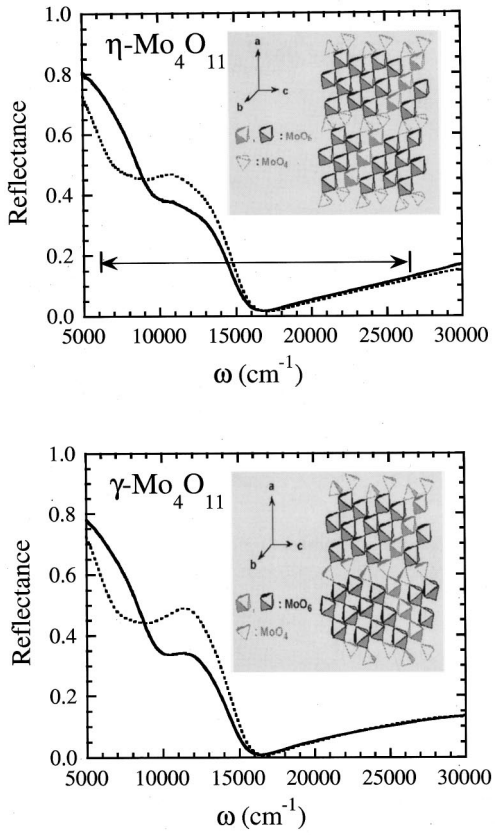

FIG. 1. Top panel: polarized room temperature reflectance spectra of η-Mo_4O_{11}. The double arrow line indicates the energy range of the optical experiments in magnetic field. Bottom panel: polarized room temperature reflectance of γ-Mo_4O_{11}. Solid lines: *b* axis; dashed lines: *c* axis. Corresponding crystal structures are shown in the insets.

bands uncross and a gap opens near Fermi level.[13]

The γ-phase material has an incommensurate transition at $T_c = 100$ K accompanied by a structural modulation similar to that of the η-phase compound ($q = 0.23b^*$).[9,10] Transport and specific heat properties show that γ-Mo_4O_{11} is also a Q2D metal below 100 K.[19] To our knowledge, there has been no report of high-magnetic field effects in γ-Mo_4O_{11}.

There have been several previous spectroscopic investigations of η- and γ-Mo_4O_{11}. Initial infrared studies by Guyot *et al.* confirmed the Q2D character of both compounds at room temperature.[20] More recently, high quality polarized far-infrared reflectance spectra of η- and γ-phase materials have been measured by McConnell *et al.*[21] In the η-phase material, a strong suppression of conductivity along the *c* axis below the 109 K CDW transition is observed, whereas a weak suppression is found along the *b* axis. Such anisotropy of the conducting *bc* plane in the far-infrared regime is more notable in η-Mo_4O_{11} than in γ-Mo_4O_{11}. Transmission measurements on both materials have complemented the aforementioned reflectance studies by focusing on changes in vibrational behavior through the CDW transitions.[22] Pump-probe experiments show that several vibrational modes couple strongly to the CDW below T_{c1}.[23] The only optical study of either material was a set of room temperature polarized reflectance measurements on γ-Mo_4O_{11}, which showed that the compound exhibits anisotropic color properties in all three directions.[24] Photoemission spectra have also been reported for η- and γ-Mo_4O_{11}.[25,26] Inverse photoemission measurements show peaks at 2.0 and 4.9 eV for the γ-phase material, attributed to e_g and t_{2g} symmetries, respectively, within a simple band model.

In the present work, we measured polarized reflectance spectra of both η- and γ-Mo_4O_{11} single crystals in the optical region as a function of temperature and examined the effect of the CDW transitions on the optical constants. To assign the nature of the observed electronic transitions and explain the effect of polarization, we carried out electronic band-structure calculations for γ-Mo_4O_{11} using the extended Hückel tight binding (EHTB) method.[27] We also explore the reflectance of η-Mo_4O_{11} in high-magnetic field in order to probe the effect of the applied field on the remaining electron and hole pockets in the CDW2 state.

II. EXPERIMENT

High-quality single crystals of both η- and γ-phase Mo_4O_{11} were prepared by standard vapor-transport techniques.[28,13] The samples used for these experiments had dimensions of $\approx 3.0 \times 2.5 \times 0.5$ mm^3, with the large face defined by the *bc* (100) plane. The surfaces were very smooth and shiny, well suited for reflectance measurements. Several single crystals were studied.

Near-normal polarized optical reflectance spectra of the samples were measured in the *bc* metallic plane with a modified Perkin-Elmer λ-900 spectrometer in the 4000–32 000 cm^{-1} energy range. Unpolarized data were also collected between 30 000 and 52 000 cm^{-1} to provide a wider range of reliable reflectance for the Kramers-Kronig extrapolation. An aluminum mirror was used as the reference for these measurements. The optical axes of the crystal were determined as those which displayed the greatest anisotropy at 300 K, and analysis of the structure showed good correspondence with the *b* and *c* directions. For each polarization, reflectance measurements were made at several temperatures above and below the CDW transitions. Temperature control was achieved using an open-flow cryostat.

The ''in-field'' single-beam reflectance (R_{SB}) spectra of η-Mo_4O_{11} in the *bc* plane were measured at 4.2 K at the National High Magnetic Field Laboratory (NHMFL) in Tallahassee, FL, using a grating spectrometer equipped with a charge coupled device (CCD) camera or Ge detector. The measurements covered the energy range 6000–26 000 cm^{-1}. The overall resolution of the spectra is ≈ 25 cm^{-1}. A resistive magnet was employed for magnetic field magnitudes up to 30 T, with the applied field always perpendicular to the conducting *bc* plane. A series of Polaroid film polarizers covered the experimental energy range along *b* and *c* polarization directions. Relative ''reflectance ratio'' (RR) spectra were obtained by taking the ratio of the single beam spectrum at a given magnetic field to the spectrum at zero field, i.e., $RR(H) = R_{SB}(H)/R_{SB}(H=0)$. Absolute reflectance spectra in the magnetic field (''in-field'' reflectance) were obtained by renormalizing the reflectance ratio with the zero field power reflectance spectrum at 10 K, i.e., $R(H) = RR(H) \times R(H=0)$.

A Kramers-Kronig analysis of the reflectance spectra was used to obtain the optical constants of η and γ-Mo_4O_{11}.

This analysis calculates the complex dielectric function

$$\tilde{\epsilon}(\omega)=\epsilon_1(\omega)+i\epsilon_2(\omega)=\epsilon_1(\omega)+\frac{4\pi i}{\omega}\sigma_1(\omega) \qquad (1)$$

from the measured reflectance and the phase shift integral.[29] Here, $\epsilon_1(\omega)$ is the real part of the dielectric function, and $\sigma_1(\omega)$ is the optical conductivity. Thus, $\epsilon_1(\omega)$ tells us how a material disperses energy, whereas $\sigma_1(\omega)$ provides information on the lossy response. In the Kramers-Kronig analysis, the high-frequency data were extrapolated as $\omega^{-1.5}$, to simulate the approach to free-electron response. After merging our low frequency data with the far-infrared data of McConnell *et al.*,[21] we extrapolated it to zero frequency with metallic Hagen-Rubens $(R(\omega)=1-A\omega^{1/2})$ behavior.

III. RESULTS

A. Room temperature spectra

The 300 K polarized optical reflectance spectra of η-Mo_4O_{11} are shown in the upper panel of Fig. 1. The spectra are characteristic of an anisotropic conducting material, with a mobile carrier response in the near infrared and two electronic transitions at higher energy. The transition centered near 12 000 cm^{-1} is superimposed on the edge of the free carrier response, and the intensity of this excitation along the *b* and *c* directions is quite different. A higher frequency transition is centered near 33 000 cm^{-1} and not shown completely in Fig. 1; the leading edge of this structure seems to be isotropic in the *bc* plane. It is notable that the overall reflectance level in the near infrared is within 1% of the far and middle infrared data of McConnell *et al.*[21]

The upper panel of Fig. 2 displays the polarized frequency-dependent conductivity, $\sigma_1(\omega)$, of η-Mo_4O_{11} at 300 K. Here, $\sigma_1(\omega)$ increases faster along *b* than along *c* towards low frequency, in agreement with the previous polarized far-infrared results.[21] The anisotropy of the low-frequency excitation is also very apparent, with bands centered at 10 000 cm^{-1} and 8500 cm^{-1} in *b* and *c* polarizations. The insets to Fig. 2 shows the partial sum rule data, calculated from the area under $\sigma_1(\omega)$, which provides information about the number of carriers participating in the optical transitions, and allows a calculation of the optical effective mass, m^*. We estimate $m^*\approx 2.2m_e$ (where m_e is the free electron mass), from the leveling off of the sum rule curve in the near infrared region. Note that the optical effective mass is heavier than the free carrier mass, which suggests the involvement of ''flat bands'' in the optical transition. The dielectric function, $\epsilon_1(\omega)$, also shows that the η-phase compound is metallic in the *bc* plane, with 300 K screened plasma frequencies (estimated from the zero-crossing of ϵ_1 in the optical regime) of 13 720 and 15 200 cm^{-1} along *b* and *c*, respectively (inset to upper panel of Fig. 2).

The 300 K polarized reflectance and optical constants of γ-Mo_4O_{11} are shown in the lower panels of Figs. 1 and 2, respectively. In essence, the results of γ-Mo_4O_{11} are similar to those of the η-phase material, which is understandable since the crystal and electronic structures are only slightly different. From the sum rule plot (inset to lower panel of Fig. 2), the effective mass $m^*\approx 3.2m_e$, larger than our estimate of m^* for the η-phase compound. The dielectric function (inset to lower panel of Fig. 2), $\epsilon_1(\omega)$, becomes negative below the screened plasma frequency (14 045 cm^{-1} along *b* and 14 524 cm^{-1} along *c*), consistent with its reported metallic character.

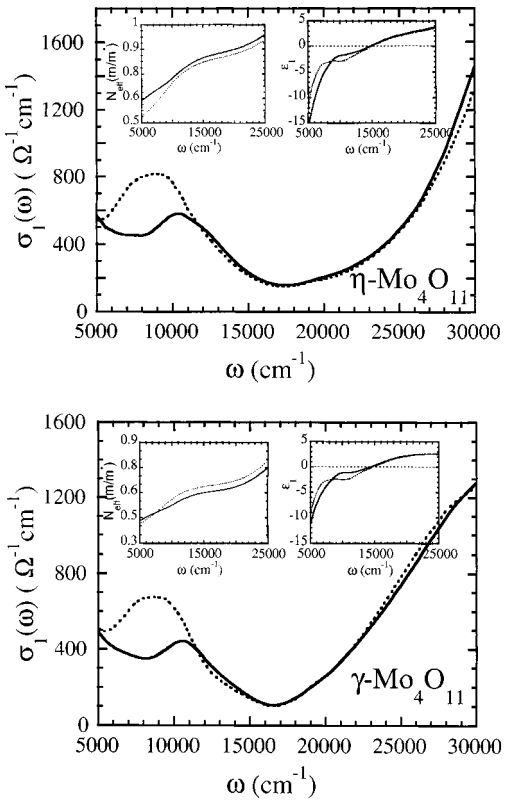

FIG. 2. Top panel: polarized room temperature conductivity of η-Mo_4O_{11}. Bottom panel: polarized room temperature conductivity of γ-Mo_4O_{11}. Left inset: sum rule results; right inset: frequency dependent dielectric constant. Solid lines: *b* axis; dashed lines: *c* axis.

B. Temperature dependence

Figure 3 shows the polarized optical conductivity of η-Mo_4O_{11} at 300, 200, 150, 120 $(T>T_{c1})$, 80 $(T_{c2}<T<T_{c1})$, and 10 K $(T<T_{c2})$. As the temperature is lowed within the normal state $(T>T_{c1})$, the residual conductivity is suppressed along both the *b* and *c* directions. The shape of the low-frequency excitation also becomes more asymmetric, especially along the *c* axis. Despite these changes, the screened plasma frequencies, $\tilde{\omega}_p$ (inset to Fig. 3), extracted from the zero-crossing of ϵ_1, are nearly constant with decreasing temperature in this range, suggesting a limited temperature dependence of the carrier concentration or effective mass in the normal state. However, on approach to T_{c1}, the low-frequency excitation and $\tilde{\omega}_p$ change noticeably, anticipating the effects of the upcoming CDW transition at 109 K. After passing from the normal state into the CDW1 state $(T_{c2}<T<T_{c1})$, the low-frequency excitation becomes more pronounced and slightly blueshifted. The asymmetry of this feature continues to increase in the CDW states as well, as shown in the 80 and 10 K spectra. Doublet character on the crest of the 12 000 cm^{-1} transition, only slightly visible

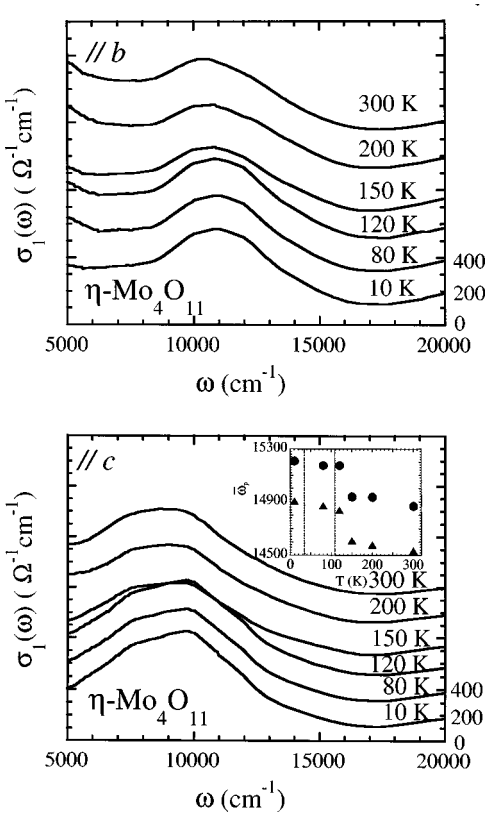

FIG. 3. Frequency dependent conductivity of η-Mo_4O_{11} in the intraband regime. Top panel: *b* axis data; bottom panel: *c* axis data. The legend is for 10 K data, and the spectra at other temperatures are offset 200 $(\Omega\ \mathrm{cm})^{-1}$ to each other. Inset: temperature dependence of the screened plasma frequency $\tilde{\omega}_p$. Triangle for *b*-axis, circle for *c*-axis. Dashed line are the 109 and 35 K transition temperatures.

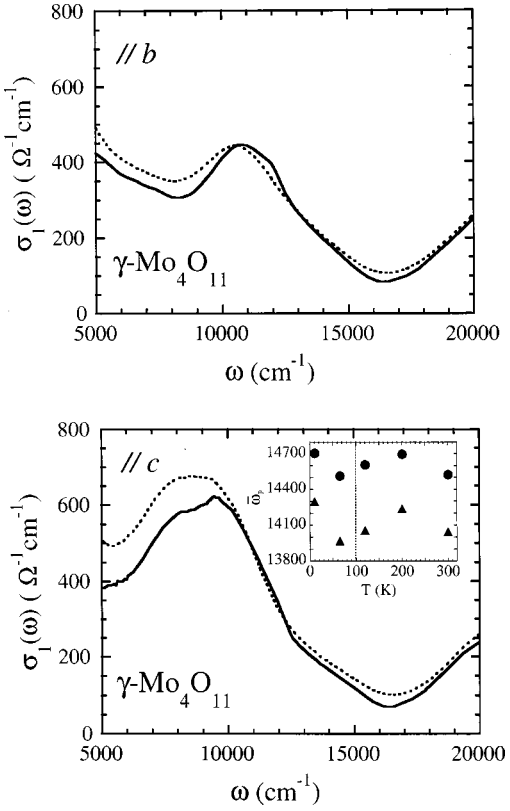

FIG. 4. Frequency dependent conductivity of γ-Mo_4O_{11} in the intraband regime. Top panel: *b*-axis; bottom panel: *c*-axis. Solid line for 10 K; dashed line for 300 K; Inset: the temperature dependence of the screened plasma frequency $\tilde{\omega}_p$. Triangle for *b*-axis; circle for *c*-axis, dashed line is the 100 K transition temperature.

along *b*, is well resolved along *c*. $\tilde{\omega}_p$ is higher in magnitude in the CDW1 state (inset to Fig 3) than in the normal state for both polarizations. Within our resolution, the optical constants of η-Mo_4O_{11} [$\sigma_1(\omega)$, $\epsilon_1(\omega)$, etc.] are not sensitive to the CDW transition at $T_{c2}=35$ K and the conductivity remains high even after a second CDW transition.

The temperature dependence of the optical spectra is much weaker in γ-Mo_4O_{11} than that in the η-phase material. Thus, only the 300 and 10 K $\sigma_1(\omega)$ of γ-Mo_4O_{11} are displayed in Fig. 4. Overall, the optical conductivity of γ-Mo_4O_{11} at 10 K is lower than that at room temperature, in agreement with the trend in the dc resistivity measurements. The transition near 12 000 cm^{-1} sharpens and becomes somewhat asymmetric with decreasing temperature. We also observe a slight blueshift of this excitation with decreasing temperature in both directions, along with the development of a very weak doublet structure. As shown in the inset to Fig. 4, $\tilde{\omega}_p$ displays a gradual change through the 100 K CDW transition and an overall blue shift going from high temperature to low temperature. This trend is different from the more abrupt jump in $\tilde{\omega}_p$ found in η-Mo_4O_{11}.

C. Electronic band structure

To interpret the optical properties of η- and γ-Mo_4O_{11} presented above, we carried out EHTB electronic structure calculations for γ-Mo_4O_{11} based on the crystal structures of Ghedira *et al.*[8] and Kihlborg,[7] and for η-Mo_4O_{11} based on the crystal structure of Kihlborg.[7] Fun *et al.* recently confirmed the $P2_1/a$ space group for γ-Mo_4O_{11},[30] as reported by Ghedira *et al.*,[8] in contrast to initial $Pnma$ identification by Kihlborg.[7] The CDW vector $q = 0.23\ b^*$, observed for η- and γ-Mo_4O_{11}, is reproduced only by the Fermi surfaces of γ-Mo_4O_{11} obtained from the crystal structures of Ghedira *et al.* Therefore, we present results of our calculations only for γ-Mo_4O_{11}. The atomic parameters used for our EHTB calculations were taken from previous work.[12]

The total density of states (DOS) calculated for γ-Mo_4O_{11} is shown in Fig. 5. The O $2p$ block bands (below -14 eV) lie about 4 eV below the bottom of the Mo $4d$ block bands. The latter can be conveniently divided into two energy regions: the lower-lying *d*-block bands between -10.2 and -7.7 eV and the higher-lying *d*-block bands between -5.7 and -2.2 eV. The Fermi level lies near the bottom of the lower *d*-block bands. The inset to Fig. 5 shows the partial DOS (PDOS) plots calculated for the four different Mo atoms [Mo(1) of the MoO_4 tetrahedra, and Mo(2), Mo(3) and Mo(4) of the MoO_6 octahedra] in the energy region of the lower-lying *d*-block bands. The sharp DOS peak around -8 eV is dominated by the Mo(1) atoms, and all four different Mo atoms contribute to the DOS below -8.5 eV. Below the Fermi level, the Mo atom contributions vary as Mo(4) $>$ Mo(3) $\gg$ Mo(2), and there is no Mo(1) contribution. Although not shown, the upper *d*-block bands do not have

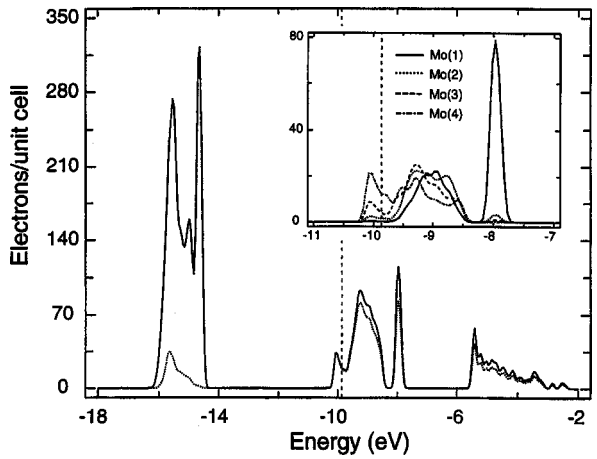

FIG. 5. DOS plots calculated for γ-Mo_4O_{11}, where the solid line refers to the total DOS, and the dashed line to the Mo 4*d* orbital contributions to the total DOS. The inset shows the PDOS plots calculated for the Mo(1), Mo(2), Mo(3) and Mo(4) atoms.

d-orbital contributions from Mo(1). Thus, as far as the MoO_6 octahedra are concerned, the lower- and higher-lying *d*-block bands correspond to the t_{2g} and e_g-block bands, respectively.

With the light polarized along a certain direction, the optical absorption involves only the occupied and unoccupied energy levels having the same wave vector aligned along the light polarization direction.[31] Therefore, to discuss the optical transitions observed with polarization along the *b* axis (*c* axis), it is necessary to find the energy levels of the lower-lying *d*-block bands along the wave vector lines parallel to the b^* direction (c^* direction), as shown in Fig. 6(a) [Fig. 7(a)]. The band dispersion relations calculated for the aforementioned wave vector lines are presented in Figs. 6(b) and 7(b), respectively. The results indicate there are more ''flat'' bands in lower-lying *d*-block bands along c^* than along b^*.

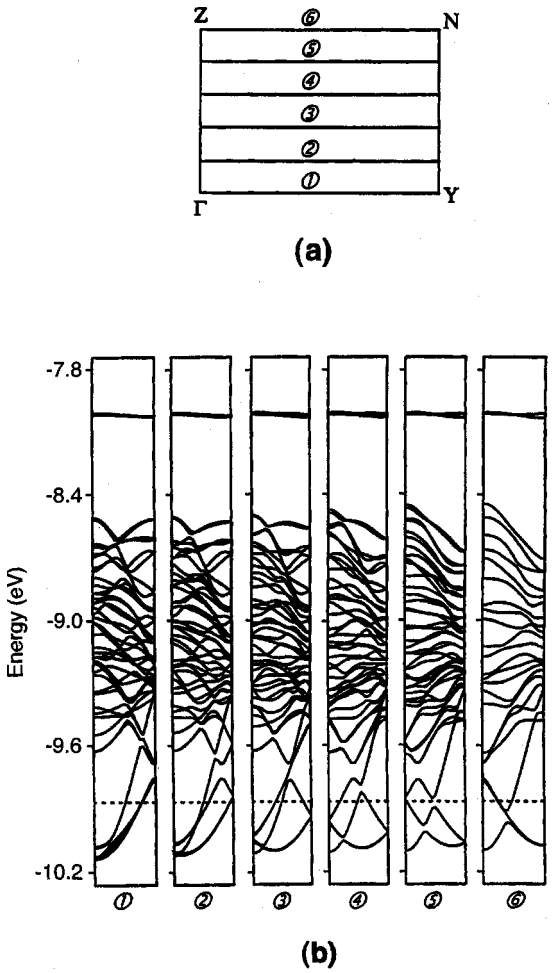

FIG. 6. (a) Six wave vector lines of the first Brillouin zone parallel to the b^* direction. (b) Dispersion relations of the lower-lying *d*-block bands along the six wave-vector line of (a).

D. Magnetic field dependence

Figure 8 displays the ''in-field'' polarized RR spectra of η-Mo_4O_{11} in different applied fields at 4.2 K. The absolute reflectance spectrum is superposed on the RR spectra to clarify which electronic transitions are changing with field. Note that our experiments in magnetic field cover a portion of the near infrared (free carrier) response, the whole intraband transition regime, and the leading edge of the charge-transfer band, as shown by the double arrow line in Fig. 1. The general trend is that the applied field increases the optical anisotropy. In the reflectance ratio spectra, a deviation from unity in the free carrier response is observed along both *b* and *c* polarizations, which apparently saturates above 10 T, as shown in the upper and lower panels of Fig. 8. In addition, the RR spectra above 14 000 cm^{-1} drops along the *b* axis, but increases along the *c* axis as the field is ramped through the 20 T transition. The ratio spectrum of 0 T (after ramping down the field) to 0 T (before ramping up the field) shows a flat line at unity for both polarizations (Fig. 8), and thus confirms that the effect of field on the RR is a real property of the material. Although the overall changes in the ratio spectra are fairly small, on the order of 2–3%, they are above our experimental noise and sensitivity level.

The optical conductivity of η-Mo_4O_{11} in magnetic field at 4.2 K is shown in the upper and lower panels of Fig. 9 for *b* and *c* axis polarizations, respectively.[32] The main magnetic field effects on $\sigma_1(\omega)$ are in the free carrier response and intraband Mo $d \rightarrow d$ transition range. Along *b*, $\sigma_1(\omega)$ drops below 9000 cm^{-1}, whereas along *c*, $\sigma_1(\omega)$ increases slightly. The effect of the magnetic field on $\sigma_1(\omega)$ is gradual, with no sharp change through the 20 T phase transition. Although RR exhibits changes above 14 000 cm^{-1}, the absolute reflectance is so small that the effect is minimized and the optical constants show no change in that regime. Comparing the upper and lower panel of Fig. 9, we find that the anisotropy in the conducting *bc* plane becomes stronger in high magnetic field. Within our resolution, the magnetic field affects mainly $\sigma_1(\omega)$, not the dispersive response.

IV. DISCUSSION

A. Temperature dependence of η- and γ-Mo_4O_{11}

The PDOS data (Fig. 5) show that excitations below 2 eV are intraband ($d \rightarrow d$) transitions involving the lower-lying *d*-block bands, and that the excitations above 4 eV are dominated by the (O $2p \rightarrow$ Mo $4d$) charge-transfer transitions. Thus, the prominent low-frequency feature in $\sigma_1(\omega)$ should be assigned to the intraband ($d \rightarrow d$) excitation within the

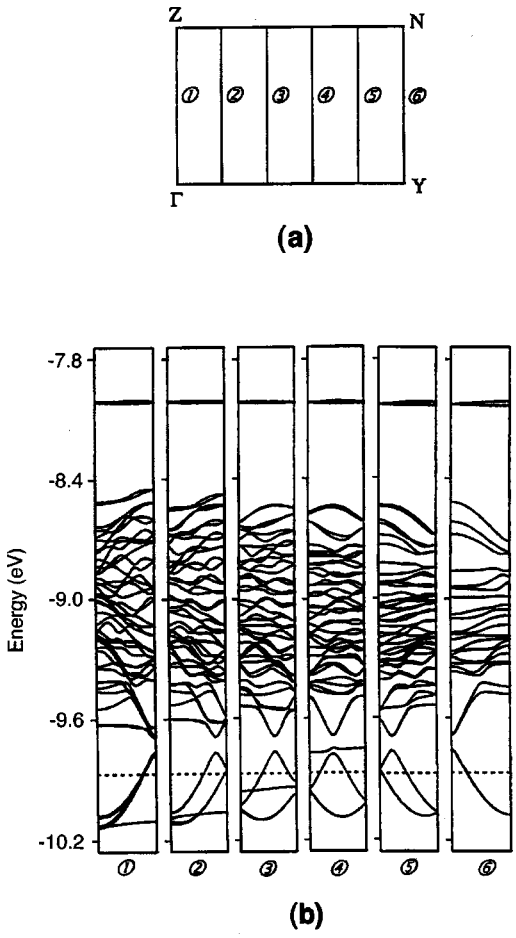

FIG. 7. (a) Six wave-vector lines of the first Brillouin zone parallel to the c^* direction. (b) Dispersion relations of the lower-lying *d*-block bands along the six wave vector line of (a).

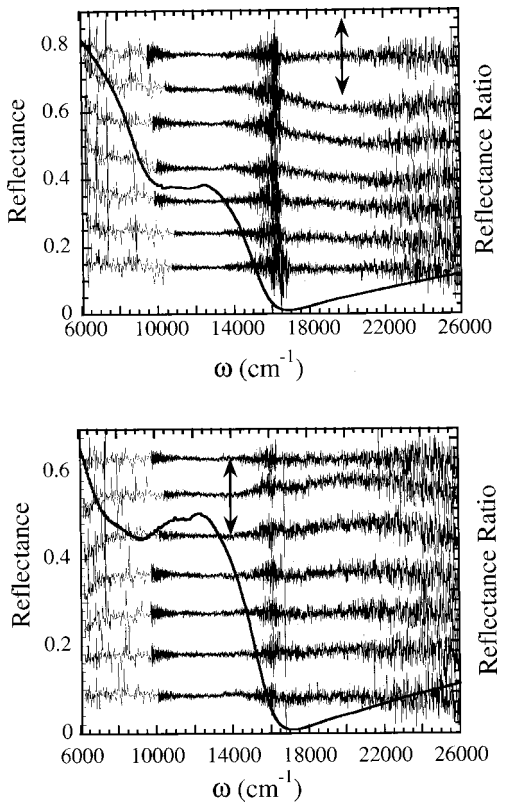

FIG. 8. Top panel: reflectance ratio spectra of η-Mo_4O_{11} in high-magnetic field along the *b* axis at 4.2 K. bottom panel: reflectance ratio spectra of η-Mo_4O_{11} in high-magnetic field along the *c* axis at 4.2 K. The ratio spectra are superimposed with the absolute reflectance spectra. The fields shown here are (from bottom to top): 5 T/0 T, 10 T/0 T, 15 T/0 T, 20 T/0 T, 25 T/0 T, 30 T/0 T and 0 T (after ramping down the field)/0 T (before ramping up the field). The spectra are offset for clarity. The double arrow indicates 4% deviation from unity.

low-lying *d*-block bands. The band centered at 33 000 cm^{-1} is most likely the O $2p \rightarrow$ Mo $4d$ charge-transfer excitation. It is improbable that the excitation centered at 33 000 cm^{-1} is related to the excitations from the filled levels of the lower-lying *d*-block bands to the empty levels of the higher-lying *d*-block bands because of the large oscillator strength of the feature.

The dc conductivities of η- and γ-Mo_4O_{11} show a Q2D character with only weak anisotropy in the bc plane.[9] In contrast, the optical response of both materials in the intraband ($d \rightarrow d$) transition regime is quite anisotropic. In particular, the excitation in the 5000–12 000 cm^{-1} region is much stronger along the *c* axis than along the *b* axis. This unusual anisotropy can be understood by comparing the band dispersion relations in Figs. 6(b) and 7(b). Recall that, for the excitation range of 5000–12 000 cm^{-1}, more ''flat'' bands are found along the c^* direction [Fig. 7(b)] than along the b^* direction [Fig. 6(b)] in the low-lying *d*-block bands. Since flat bands lead to high DOS, the excitation will be more intense for the *c*-axis polarization. This also explains why the oscillator strength of the intraband ($d \rightarrow d$) transition is stronger along *c* than along *b*. The far-infrared spectra of η-Mo_4O_{11} indicate that the optical anisotropy of η-Mo_4O_{11} continues into the lower energy region.[21] Discrepancies between dc and optical conductivities such as mentioned above have been found in other bronzes as well.[33,34]

Figure 3 shows that, for temperatures above T_{c1} (109 K), the intensity of the intraband ($d \rightarrow d$) transition of η-Mo_4O_{11} remains fairly constant, whereas the overall background of the spectrum decreases as the temperature is lowered. This behavior indicates a loss of mobile carriers.[35] In addition, the spectra of η-Mo_4O_{11} at 120 and 80 K are similar, suggesting that there are strong CDW fluctuations above 109 K.[36] This is consistent with the observation of CDW fluctuations by x-ray diffraction experiments at temperatures above T_{c1} (Ref. 10) and with far-infrared results.[22] The effect of the CDW transition on the intraband ($d \rightarrow d$) excitation is more noticeable along *c* than along *b*, and manifest in a more pronounced doublet structure along *c*. Far-infrared reflectance measurements confirm the enhanced sensitivity of the *c*-axis response to CDW formation.[21] The temperature dependence of the $d \rightarrow d$ intraband transition and the plasma frequency is likely related to the fine structure developing in the DOS through the CDW1 transition at 109 K. In a CDW system, the instability due to interactions between conduction electrons and phonons leads to opening of the CDW gap around the Fermi level, which modifies the fine structure of the conduction band and Fermi surface. In the case of Mo_4O_{11}, the modified band structure and Fermi surface in the CDW states affect the intraband transition because the $d \rightarrow d$ transition involves electrons close to the Fermi energy.

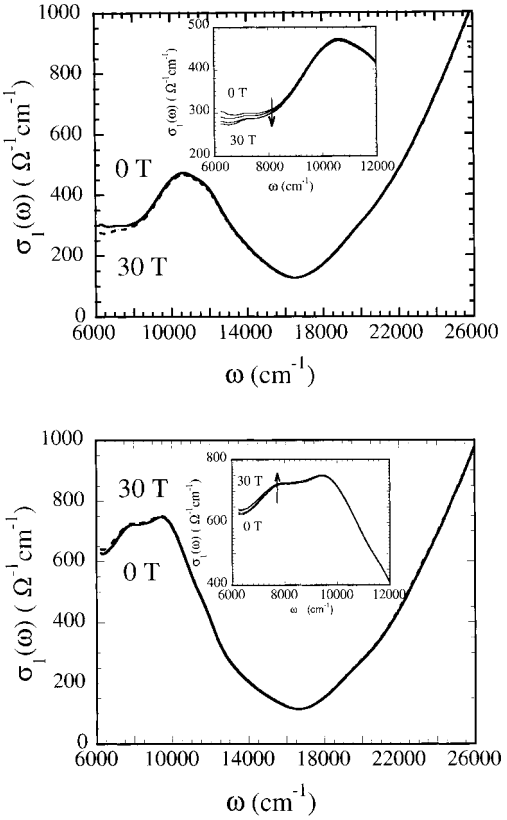

FIG. 9. Top panel: Optical conductivity of η-Mo_4O_{11} in high-magnetic field along the *b* axis at 4.2 K. bottom panel: optical conductivity of η-Mo_4O_{11} in high-magnetic field along the *c* axis at 4.2 K.

We observe that $\tilde{\omega}_p$ of η-Mo_4O_{11} displays a sharp increase when the temperature is lowered through T_{c1} at 109 K. Since $\tilde{\omega}_p^2 = 4\pi ne^2/m^*$, the screened plasma frequency is dependent on the carrier concentration n and the effective mass m^*. The carrier concentration decreases by about 70% (Ref. 11) while the $\tilde{\omega}_p$ increases slightly after the first CDW transition, suggesting that the optical effective mass of η-Mo_4O_{11} must decrease dramatically. This is in line with the estimated $m^* \approx 10m_0$ in the normal phase[11] compared to $m^* \approx 0.1m_0$ in the CDW2 state ($T < T_{c2}$).[13] The second CDW transition of η-Mo_4O_{11} at 35 K shows little effect on the optical conductivity in agreement with x-ray diffraction[10] and far-infrared reflectance measurements.[21]

In contrast to the behavior of η-Mo_4O_{11}, the CDW formation in γ-Mo_4O_{11} at 100 K has only a weak effect on the optical conductivity, and $\tilde{\omega}_p$ of γ-Mo_4O_{11} decreases slightly as the temperature is lowered through the CDW transition. These observations imply that the 109 K CDW in η-Mo_4O_{11} induces a stronger structural change than does the 100 K CDW in γ-Mo_4O_{11}. Strong electron-phonon coupling drives a CDW transition, and thus a soft lattice is conducive for CDW formation.[37] That the optical transition is more strongly affected by the 109 K CDW of η-Mo_4O_{11} than by the 100 K CDW of γ-Mo_4O_{11} therefore implies that η-Mo_4O_{11} has a softer lattice than does γ-Mo_4O_{11}. Specific heat measurements indicate that this is indeed the case.[19] At the same time, η-Mo_4O_{11} shows negative thermal expansion in the lattice spacing *b* and *c* below T_{c1} (Ref. 38) although it has smaller compressibility than γ-Mo_4O_{11} at room temperature.[39] The softer lattice may also explain the occurrence of two CDW transitions in η-Mo_4O_{11}, as opposed to one transition in γ-Mo_4O_{11}.

In overall spectroscopic response, η- and γ-Mo_4O_{11} bear a notable resemblance to other oxide bronzes that show CDW transitions. The quasi-one-dimensional (Q1D) blue bronze $K_{0.3}MoO_3$ and purple bronze $Li_{0.9}Mo_6O_{17}$ undergo a CDW transition at low temperature, and their optical responses show a strong anisotropy reflecting the Q1D character of their electronic structures.[33,34] For the Q2D purple bronzes, $Na_{0.9}Mo_6O_{17}$ and $K_{0.9}Mo_6O_{17}$, the optical responses are isotropic in the conducting plane due to the fact that the metallic layers of these compounds have a trigonal symmetry. Thus, the anisotropy of Mo_4O_{11} reported here is unexpected. All of these molybdenum bronzes, including η- and γ-Mo_4O_{11}, have an isotropic electronic transition at energies above 4 eV, which is attributed to the (O $2p \rightarrow$ Mo $4d$) charge-transfer excitation. Compared with η-Mo_4O_{11}, the aforementioned bronzes show a much weaker temperature dependence of the optical spectra and hence are similar to γ-Mo_4O_{11}. In addition, as found for γ-Mo_4O_{11}, the plasma frequencies of the Q2D purple bronzes $Na_{0.9}Mo_6O_{17}$ and $K_{0.9}Mo_6O_{17}$ decrease through CDW transition. These purple bronzes exhibit a commensurate CDW transition, at 88 K for $Na_{0.9}Mo_6O_{17}$ and 120 K for $K_{0.9}Mo_6O_{17}$.

The Q2D material $2H$-$TaSe_2$, like η-Mo_4O_{11}, also displays two CDW transitions at low temperature (122 and 90 K). The first CDW transition at 122 K is incommensurate and the second transition is very weak. As for $2H$-$TaSe_2$, although spectroscopic studies did not show any strong temperature dependence in the optical regime, the far-infrared results[40] seem to suggest that a CDW gap is partially open. However, the CDW transitions of $2H$-$TaSe_2$ are not caused by Fermi surface nesting, but by a clustering of the metal atoms.[41] Recently, the transport and thermopower studies on Q2D monophosphate tungsten bronzes, $(PO_2)_4(WO_3)_{2m}$ ($m = 4,6$), show that these materials exhibit two incommensurate CDW transitions at low temperature,[42] and have an anisotropic thermopower in the conducting plane in the CDW states. Optical investigations on these tungsten bronzes will provide a more general picture of the CDW transitions in Q2D transition metal oxides.

B. Magnetic field dependence of η-Mo_4O_{11}

A majority of the room temperature Q2D Fermi surface of η-Mo_4O_{11} is nested through the CDW1 transition at 109 K.[43] According to recent photoemission data on γ-Mo_4O_{11} below the density wave transition, the remaining pockets are fairly anisotropic.[26] A similar result is anticipated for the CDW1 phase of η-Mo_4O_{11}, but the CDW2 transition at 35 K leaves very small, highly two-dimensional electron and hole pockets.[44] The exact shape and size of these pockets (and their field dependence) is not known.

In general, the shape of 2D Fermi surface pockets is sensitive to an applied magnetic field. However, the pockets in the CDW2 state of η-Mo_4O_{11} are so small that the overall field dependence should be weak. Theoretical calculations of magnetic field effects on Q1D CDW systems indicate that

the CDW is sensitive to both orbital and Pauli effects of the field.[45] Here, the transverse magnetic field constrains the electron motion and therefore improves the Fermi surface nesting.[45] An extension of this sort of theoretical model to Q2D systems would be useful, although even without such a model, the qualitative effects of the field can be discussed. In Q2D systems, the magnetic field dependence of the nesting vector is likely more complicated, giving rise to some unusual transport properties, such as a hysteresis effect.[13,46] The CDW nesting vector of η-Mo_4O_{11} is further complicated by additional CDW periodicity above the 19 T Landau transition, since the quantum limit state of 2D electrons is a CDW state with a large gap at the Fermi level.[47] Magnetic breakdown effects may also play a role in shaping the Fermi surface, as observed by Shubnikov-de Haas experiments in other CDW systems, such as 2H-$NbSe_2$ and purple bronze ($TlMo_6O_{17}$).[48,49] In magnetic breakdown, the magnetic energy is sufficient to overcome a small gap between different Fermi pockets and the carriers can move between different orbits. In η-Mo_4O_{11}, the applied field may allow the string of 2D pockets, which lie on a line along b^* (or c^*) (Fig. 7 of Ref. 44) to become ''reconnected,'' causing a one-dimensional-like Fermi surface to be restored. In this scenario, the pockets need not be completely connected in order to make the material more anisotropic. The anisotropic nature of the pockets and the overall Fermi surface could also give two energy scales (along b^* and c^*) for magnetic breakdown.

The aforementioned arguments all predict a more anisotropic Fermi surface in magnetic field, in general agreement with the increased anisotropy of η-Mo_4O_{11} optical properties at 4.2 K and 30 T (Fig. 9). The stronger field-induced anisotropy in the optical conductivity along b is consistent with the preferential nesting direction as well. However, the CDW energy gaps are small in η-Mo_4O_{11}, so the associated magnetic breakdown would be a fairly low-energy process. Thus, the field-dependent near-infrared optical response of η-Mo_4O_{11} is unexpected and not likely to be directly related to the magnetic breakdown. Indeed, the Fermi surface arguments do not seem to apply to the energy scale probed in our measurements. Nevertheless, the intraband transition of η-Mo_4O_{11} is sensitive to the band shape and joint density of states, which could be modified by field-induced merging of pockets at low field. As a result, the spectral properties may be indirectly sensitive to a magnetic breakdown driven Fermi surface modification thereby increasing the 1D character of the material. Electronic band and lattice effects provide other possible (higher energy) mechanisms. Further investigation is in progress.

V. CONCLUSION

We have measured the polarized optical reflectance of two CDW materials, η- and γ-Mo_4O_{11}, as a function of temperature and magnetic field. A fairly strong anisotropic optical response in the conducting bc plane was observed for both materials in the electronic excitations below 2 eV. This anisotropy arises from the intraband ($d \rightarrow d$) transitions, and is explained nicely by the band dispersion relations calculated for the wave vector directions parallel to the b^* and c^* directions. The 109 K CDW transition in η-Mo_4O_{11} has a stronger effect on the optical properties than does the 100 K CDW transition in γ-Mo_4O_{11}. This must be related to the fact that η-Mo_4O_{11} has a less rigid lattice than does γ-Mo_4O_{11}.

Our temperature-dependent optical studies provide a fundamental ground work for optical investigations of η-Mo_4O_{11} in high-magnetic field. Such measurements are of interest to correlate the dielectric response with recent magnetotransport data and probe the nature of the high-field state. We find the main effect of the applied field is to increase the anisotropy of the free carrier and intraband response, thus giving the high-field state more low-dimensional character. This may be related to magnetic breakdown, although the energy scale is unexpected.

ACKNOWLEDGMENTS

Work at SUNY-Binghamton was supported by the Division of Material Research, National Science Foundation under Grant No. 9623221, and by the Division of Materials Science, Basic Energy Science at the U.S. Department of Energy under Grant No. DE-FG02-99ER45741. Work at North Carolina State University was supported by the Division of Materials Science, Basic Energy Sciences, U. S. Department of Energy under Grant No. DE-FG05-86ER45259. The measurements at high magnetic field were performed at the National High Magnetic Field Laboratory, in Tallahassee, Florida, which is supported by NSF Cooperative Agreement No. DMR-9527035 and by the State of Florida. S. Chowdhary thanks the Dean's Office of SUNY-Binghamton for financial support. We gratefully acknowledge C.C. Homes and A.W. McConnell for generous access to their far-infrared data and many useful discussions.

[1] *Low Dimensional Electronic Properties of Molybdenum Bronzes and Oxides*, edited by C. Schlenker (Dordrecht, Kluwer, 1989).
[2] *Oxide Bronzes*, edited by M. Greenblatt [Int. J. Mod. Phys. B, **7** Nos. 23 & 24, (1993)].
[3] E. Canadell, Chem. Mater. **10**, 2770 (1998).
[4] E. Canadell and M.-H. Whangbo, Phys. Rev. B **43**, 1894 (1991).
[5] G. Grüner, *Density Waves in Solids* (Addison-Wesley, New York, 1994).
[6] E. Canadell and M.-H. Whangbo, Int. J. Mod. Phys. B **7**, 4005 (1993).
[7] L. Kihlborg, Ark. Kemi **21**, 365 (1963).
[8] M. Ghedira, H. Vincent, and M. Marezio, J. Solid State Chem. **56**, 66 (1985).
[9] H. Guyot, C. Escribe-Filippini, G. Fourcaudot, K. Konaté, and C. Schlenker, J. Phys. C **16**, L1227 (1983).
[10] H. Guyot, C. Schlenker, J. P. Pouget, R. Ayroles, and C. Roucau, J. Phys. C **18**, 4427 (1985).
[11] M. Sasaki, G. X. Tai, S. Tamura, and M. Inoue, Phys. Rev. B **47**, 6216 (1993).
[12] E. Canadell, M.-H. Whangbo, C. Schlenker, and C. Escribe-Filippini, Inorg. Chem. **28**, 1466 (1989).
[13] S. Hill, S. Valfells, S. Uji, J. S. Brooks, G. J. Athas, P. S. Sandhu,

J. Sarrao, Z. Fisk, J. Goettee, H. Aoki, and T. Terashima, Phys. Rev. B **55**, 2018 (1997).
[14] M. Inoue, S. Ôhara, S. Horisaka, M. Koyano, and H. Negishi, Phys. Status Solidi B **148**, 659 (1988).
[15] C. Schlenker, J. Dumas, C. Escribe-Filippini, H. Guyot, J. Marcus, and G. Fourcaudot, Philos. Mag. B **52**, 643 (1985).
[16] S. Hill, S. Uji, M. Takashita, C. Terakura, T. Terashima, H. Aoki, J. S. Brooks, Z. Fisk, and J. Sarrao, Phys. Rev. B **58**, 10 778 (1998).
[17] M. Sasaki, N. Miyajima, H. Negishi, S. Negishi, M. Inoue, H. Kadomatsu, and G. Machel, Solid State Commun. **109**, 357 (1999).
[18] M. Sasaki, Y. Kawamura, W. X. Gao, H. Negishi, and M. Inoue, Synth. Met. **103**, 2662 (1999).
[19] H. Guyot, C. Schlenker, G. Fourcaudot, and K. Konaté, Solid State Commun. **54**, 909 (1985).
[20] H. Guyot, E. A. Khoury, J. Marcus, and C. Schlenker, Solid State Commun. **79**, 307 (1991).
[21] A. W. McConnell, B. P. Clayman, C. C. Homes, M. Inoue, and H. Negishi, Phys. Rev. B **58**, 13 565 (1998).
[22] Z. Zhu, J. L. Musfeldt, Y. J. Wang, J. Sarrao, Z. Fisk, H. Negishi, and M. Inoue, Synth. Met. **103**, 2238 (1999).
[23] K. Kenji, M. Hase, H. Harima, S. Nakashima, M. Tani, K. Sakai, H. Negishi, and M. Inoue, Phys. Rev. B **58**, 7484 (1998).
[24] M. Okachi, M. Shimoda, and K. Yagisawa, J. Mater. Sci. Lett. **7**, 599 (1988).
[25] M. Nakatake, M. Tamura, H. Namatame, M. Taniguchi, Y. Ueda, K. Morikawa, T. Mizokawa, A. Fujimori, H. Negishi, and M. Inoue, J. Electron Spectrosc. Relat. Phenom. **78**, 485 (1996).
[26] A. Terrasi, M. Marsi, H. Berger, F. Gauthier, L. Forro, G. Margaritondo, R. J. Kelley, and M. Onellion, Z. Phys. B: Condens. Matter **100**, 493 (1996).
[27] M.-H. Whangbo and R. Hoffmann, J. Am. Chem. Soc. **100**, 6093 (1978).
[28] H. Negishi, T. Miyahara, and M. Inoue, J. Cryst. Growth **144**, 320 (1994).
[29] F. Wooten, *Optical Properties of Solids* (Academic Press, New York, 1972).
[30] H.-K. Fun, P. Yang, M. Sasaki, M. Inoue, and H. Kadomatsu, Acta Crystallogr., Sect. C: Cryst. Struct. Commun. **55**, 841 (1999).
[31] H.-J. Koo, M.-H. Whangbo, J. Dong, I. Olejniczak, J. L. Musfeldt, J. A. Schlueter, and U. Geiser, Solid State Commun. **112**, 403 (1999).
[32] Kramers-Kronig analysis calculates optical constants via phase shift and dispersion relations, which is related to the reflectivity by well-known equations (Ref. 29).
[33] L. Degiorgi, P. Wachter, M. Greenblett, W. H. McCarroll, K. V. Ramanujachary, J. Marcus, and C. Schlenker, Phys. Rev. B **38**, 5821 (1988).
[34] G. Travaglini, P. Wachter, J. Marcus, and C. Schlenker, Solid State Commun. **37**, 599 (1981).
[35] The optical conductivity of η-Mo_4O_{11} can be fit with two Drude models, which implies that two different types of mobile carriers exist in the material. Here, the carriers with less mobility disappear as the temperature is lowered. Two types of mobile carriers with different mobility are also observed in 2H-$TaSe_2$. [see Vescoli *et al.*, Synth. Met. **103**, 2655 (1999)].
[36] R. Moret and J. P. Pouget, *Crystal Chemistry and Properties of Materials with Quasi-One-Dimensional Structures* (Reidel, The Netherlands, 1986).
[37] M.-H. Whangbo, D.-K. Seo, and E. Canadell, in *Physics and Chemistry of Low-Dimensional Inorganic Conductors*, edited by C. Schlenker, M. Greenblatt, J. Dumas, and S. V. Smaalen (Plenum, New York, 1996).
[38] Y. Koroiwa, the lattice spacing b and c of η-Mo_4O_{11} show minima around T_{c1}, below which it shows a negative thermal expansion by -0.004% and -0.009%, respectively (private communication).
[39] M. Koyano, S. Ôhara, H. Negishi, M. Sasaki, M. Inoue, M. Nomura, and H. Fujiwara, Phys. Status Solidi B **147**, 559 (1988).
[40] V. Vescoli, L. Degiorgi, H. Berger, and L. Forro, Phys. Rev. Lett. **81**, 453 (1998).
[41] M.-H. Whangbo and E. Canadell, J. Am. Chem. Soc. **114**, 9587 (1992).
[42] C. Hess, C. Schlenker, J. Dumas, M. Greenblatt, and Z. S. Teweldemedhin, Phys. Rev. B **54**, 4581 (1996).
[43] E. Canadell and M.-H. Whangbo, Chem. Rev. **91**, 965 (1991).
[44] M. Sasaki, N. Miyajima, H. Negishi, W.-X. Gao, M. Inoue, H. Kadomatsu, G. Machel, H. Nojiri, and M. Motokawa, J. Phys. Soc. Jpn. **68**, 539 (1999).
[45] D. Zanchi, A. Bjeliš, and G. Montambaux, Phys. Rev. B **53**, 1240 (1996).
[46] M. Koyano, S. Ôhara, S. Horisaka, H. Negishi, M. Inoue, S. Takeyama, and N. Miura, Solid State Commun. **71**, 317 (1989).
[47] D. Yoshioka and H. Fukuyama, Surf. Sci. **98**, 272 (1980).
[48] M. Naito, S. Tanaka, and N. Miura, in *Physics in High Magnetic Fields*, edited by S. Chikazumi and N. Miura (Springer-Verlag, Berlin, 1981).
[49] X. Qin, J. Shi, H. Gong, M. Tian, J. Wei, H. Chen, and D. Tian, Phys. Rev. B **53**, 15 538 (1996).